Magnetic Circular Dichroism of Nonaromatic Cyclic π-Electron Systems. 5.[1] Biphenylene and Its Aza Analogues[†]

Jörg Fleischhauer,[§] Udo Höweler,[⊥] Jens Spanget-Larsen,[||] Gerhard Raabe,[§] and Josef Michl*,[‡]

Department of Chemistry and Biochemistry, University of Colorado, Boulder, Colorado, Institut für Organische Chemie, RWTH−Aachen, Prof. Pirlet-Str. 1, D-52056 Aachen, Germany, and Department of Life Sciences and Chemistry, P.O. Box , DK-4000 Roskilde, Denmark

Received: December 11, 2003; In Final Form: January 20, 2004

The algebraic form of the perimeter model for nonaromatic cyclic π-electron systems developed in parts 1−4 of this series is used to analyze the previously reported magnetic circular dichroism (MCD) of biphenylene (**1**) and its aza analogues, to classify its excited states, and to relate them to those of other nonaromatic cyclic π systems. The observed MCD signs are interpreted in terms of relative sizes of orbital energy differences and the resulting configuration energy ordering. These require deviations from the alternant pairing associated with the simplest classical description, which are attributed to the increased negative magnitude of the diagonal resonance integrals in the four-membered ring. The interpretation of the UV and MCD spectra of **1** is confirmed by the observed effects of aza substitution, and predictions for other types of substitution follow. The magnetic field induced state mixing deduced from the perimeter model is supported by computations by the linear combination of orthogonalized atomic orbitals (LCOAO), time-dependent density functional theory (TD DFT), and symmetry-adapted cluster configuration interaction (SAC-CI) methods.

Cyclic π-electron chromophores are known in vast numbers and a bewildering variety of structures. Organizing and classifying them in a way that permits an overarching description of their electronic states has long appeared as an attractive goal. The classical perimeter model[2,3] has accomplished this objective for those cyclic π-electron systems that are aromatic in the sense that they can be formally derived from a $(4N + 2)$-electron perimeter (see part 1[4] for details concerning the classification of cyclic π-electron systems that we have introduced for the purposes of electronic spectroscopy and magnetic circular dichroism, MCD). The perimeter model provided a correlation of low-lying electronic states within a multitude of these structures and offered a qualitative understanding of the energies, intensities, and polarization directions of their electronic transitions based on inspection of molecular structural formulas. In its updated form,[5−7] it permitted the prediction and rationalization of peak signs and magnitudes in MCD as well. We believe that such simple conceptual models conserve their value at present and, if anything, will enhance it in the future, as ab initio numerical computations become increasingly able to predict experimental data accurately. Although it may be very useful, the replacement of a measurement by an accurate calculation does not provide much understanding in itself.

The first four papers of the present series[1,4,8,9] described a similarly simple algebraic model for absorption and MCD spectra of nonaromatic cyclic π-electron systems, i.e., those derivable from a $4N$-electron perimeter. MCD spectra are of particular interest to us. Whereas the perimeter model for the absorption and MCD of aromatic molecules has been thoroughly tested on numerous aromatic hydrocarbons, their derivatives, and heterocyclic analogues,[10] the perimeter model for nonaromatic molecules has so far undergone only limited testing,[1] some of it in its preliminary form.[11] It has no ambitions in the direction of predicting accurate state energies, but we hope that the energy and intensity of the first few electronic transitions can be mutually correlated and understood similarly as has been the case for those derived from $(4N + 2)$-electron perimeters.[2,3,5−7,10] Given the experimental energies, the model should predict the MCD signs and offer an understanding of their origin in terms of state mixing by the magnetic field. In the following papers of this series, we examine its performance on a series of cyclic π-electron systems derived from a $4N$-electron perimeter. We start with a known problem case, biphenylene.[10] As shown in formula **1**, this hydrocarbon can be derived from a [12]annulene perimeter by introducing two cross links.

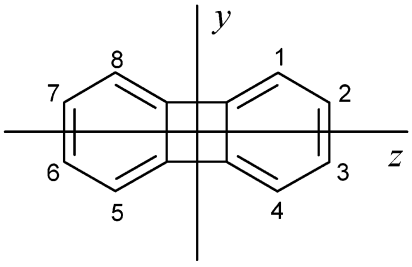

1

The testing of the model consists of two steps. The first is a comparison of the predicted MCD signs and trends with those observed. This has always been possible, and indeed it is how the performance of the perimeter model for aromatic compounds was evaluated initially.[10] Nowadays, however, a second step is also possible: computers and algorithms are powerful enough

[†] Part of the special issue "Fritz Schaefer Festschrift".

* Author to whom correspondence may be addressed. E-mail: michl@eefus.colorado.edu.

[‡] University of Colorado.

[§] Rheinisch-Westfaelische Technische Hochschule Aachen.

[||] Roskilde University.

[⊥] Present address: Organisch-Chemisches Institut, Westfälische Universität Münster, D-48149 Münster, Germany.

10.1021/jp037806g CCC: $27.50
Published on Web 02/25/2004

to permit credible ab initio calculations on molecules of an appropriate size, permitting a verification of the intermediate results appearing in the model. On selected examples, one can thus compare the nature of the excited state wave functions, the origin of the transition moments, and in the case of MCD spectroscopy, also the individual magnetic field induced state-mixing terms in the sum over states[12] invoked in the formulation[1,4,8,9] of the perimeter model (we use the formulas for A, B, and C terms given in part 1;[4] note that a positive MCD peak corresponds to a negative *B* term). Such a check was recently run for a series of aromatic derivatives and hetero analogues of benzene,[13] using the ab initio symmetry-adapted cluster configuration interaction (SAC-CI)[14] description of electronic states, and it was found that the description of magnetically induced state mixing provided by the perimeter model indeed agrees with that provided by ab initio theory. The sum-over-states formulation of MCD properties has obvious disadvantages, particularly in ab initio calculations, where the summation is over a very large number of states. However, in a simple algebraic approach adopted in the perimeter model, the sum is short and the formulation has the advantage of offering immediate insight into qualitative effects of those perturbations of molecular structure that change transition energies and moments.

We test the performance of the perimeter model for **1** and two of its aza derivatives by comparing its predictions with (i) observed spectra and (ii) results of calculations with the linear combination of orthogonalized atomic orbitals (LCOAO),[15] time-dependent density functional theory (TD DFT),[16] and SAC−CI[13,14] methods. Since the perimeter model also makes specific predictions for substitution patterns needed to reverse MCD signs or modify MCD intensities, it is subject to further future verification.

Method of Calculation

Two modifications of the original[17] complete neglect of differential overlap/spectroscopic (CNDO/S) method were used, one due to Baumann and Oth[18] and the other to Dick and Hohlneicher.[19] Both of these calculations and also the LCOAO calculation[15] used the experimental geometry[20] of **1**, and this was used for the LCOAO calculations on aza derivatives of **1** as well. The modified neglect of diatomic overlap correlated (MNDOC) calculation[21] used an MNDO-optimized geometry of **1**.

TD DFT calculations used the B-P86 functional[22] and the TZVP basis set[23] and were performed at a B-P86/TZVP optimized geometry of **1**.

Hartree−Fock (HF) and SAC-CI calculations used Dunning's DZP basis set[24] and were performed at MP2/6-31+G*-optimized geometries. The active space in SAC-CI calculations consisted of 20 occupied and 20 virtual orbitals (20/20) unless specified otherwise.

The programs employed were Gaussian 98[25] and SAC-CI[13] for ab initio computations of ground state and excited state properties, respectively. Turbomole[26] was used for density-functional calculations.

Results and Discussion

In the following, we first summarize the experimental and computational information available on the low-energy electronic states of **1** and its aza analogues and describe them in terms of MO configurations. Subsequently, we analyze the excited states of **1** in terms of the perimeter model, which permits us to rationalize the results by inspection of its Hückel orbitals, and we examine the degree to which the predictions of the model agree with the results of LCOAO, TD DFT, and SAC-CI calculations. Finally, we discuss briefly the effects of perturbations by the aza nitrogens in 1,8-diazabiphenylene (**1,8-N-1**) and 2,7-diazabiphenylene (**2,7-N-1**) and formulate predictions for other derivatives of **1**.

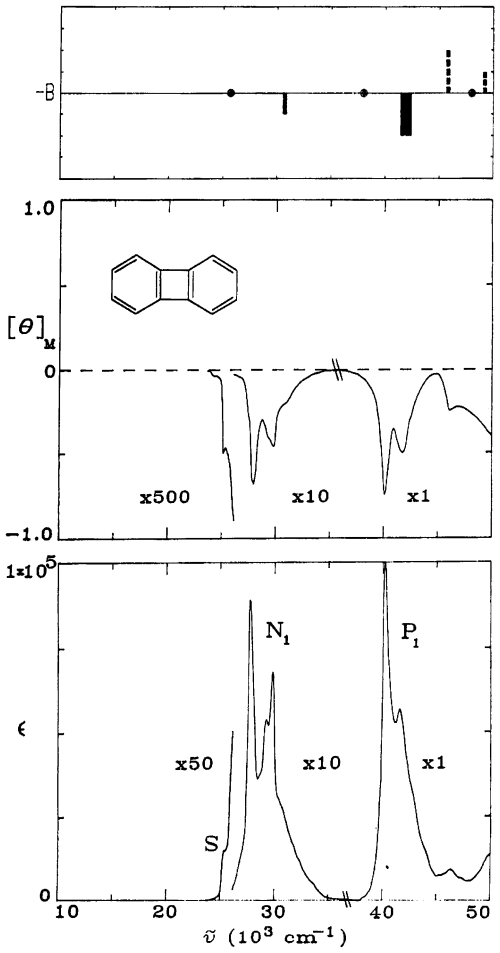

Figure 1. The absorption (bottom) and MCD (top) spectra of **1**, adapted from refs 29 and 31 (in ref 31, factor ×10 is missing in the central part of the MCD spectrum). Results of an LCOAO calculation are shown on top. The $-B$ value is shown by bars (short, $|B| < 1$; medium, 1−5; long, > 5, in units of 10^{-3} Bohr magneton Debye^2/cm^{-1}). Solid bars indicate *z*-polarized, and broken bars indicate *y*-polarized transitions. Bar thickness gives the oscillator strength (thin, $f < 0.1$; medium, 0.1−1.0; thick, >1.0). Forbidden transitions are indicated by dots.

Electronic States of Biphenylene. *General Considerations.* The measurement and interpretation of the electronic spectrum of **1** (Figure 1) have been the subject of considerable attention,[27−33] and it has been long recognized[28] that the low-energy electronic states of this 4*N*-electron perimeter species do not fit the classical Platt−Moffitt scheme[2] characteristic of (4*N* + 2)-electron perimeter aromatic hydrocarbons.

For instance, the lowest-energy singlet transition of this D_{2h} molecule, located at ∼24 000 cm^{-1}, is not only weak, as is frequently the case in benzenoid hydrocarbons, but it is also symmetry forbidden, in sharp contrast to D_{2h} benzenoid analogues such as naphthalene. Polarized absorption measurements in stretched polymer sheets showed that all of the significant absorption intensity observed in **1** up to about 47 000 cm^{-1} is long-axis (*z*) in-plane polarized.[28,29] A subsequent measurement[30] revealed a short-axis (*y*) in-plane polarized transition at ∼50 000 cm^{-1}. The MCD spectrum of **1** (Figure 1) initially presented a puzzle in that all three *B* terms observed

down to ~200 nm, at ~24 000, ~28 000, and ~40 000 cm^{-1}, are positive.[29] Their relatively high MCD intensity contradicted a theorem[34] according to which uncharged alternant hydrocarbons have vanishing MCD in the standard π-electron PPP approximation and suggested that the presence of a four-membered ring is somehow responsible for a partial breakdown of perfect alternant pairing symmetry ("pseudoparity"), i.e., of the distinction[35] between "plus" and "minus" states. The breakdown is clearly not complete, since in two-photon absorption spectra[32] transitions into the plus states are only weakly present, even when allowed by geometrical symmetry.

Alternant pairing symmetry holds in the classical model because the next-nearest neighbor resonance integrals β_{13} are set equal to zero and because the effective electronegativity of all carbon atoms is the same.[35] Semiempirical all-valence-electron theories such as CNDO/S describe the situation very poorly in that they do not reproduce the alternant pairing properties even where experiments demand that they should,[36] because they attribute far too large a negative value to β_{13}. Explicit orthogonalization of the AOs and introduction of penetration integrals are an obvious remedy, but the fine balance needed to reproduce properly the observed alternant properties of benzenoid hydrocarbons and the MCD spectrum of **1** was not initially achieved in the π-electron approximation.[29] A subsequently developed procedure, the LCOAO method, described well the observed pairing properties of benzenoid hydrocarbons and has reproduced the most prominent MCD signs of **1**.[15] This procedure is parametrized in such a manner that the resonance integral β_{13} between Löwdin-orthogonalized atomic orbitals just vanishes in the six-membered ring of benzene owing to mutual cancellation of "through-space" and "through delocalized wing" contributions.[5] In a four-membered ring, as encountered in **1**, the distance between next-nearest neighbors is smaller, the through-space contribution dominates, and β_{13} is weakly negative (still an order of magnitude smaller than β_{12}). In a planar eight-membered ring, the opposite holds, and β_{13} is weakly positive.

In one of the investigations[31] of the MCD and polarized spectra of **1**, it has been claimed that a weak short-axis polarized transition is present at ~38 000 cm^{-1}. Such *y*-polarized intensity was absent in the three previously recorded stretched-sheet spectra of **1**,[28−30] at least two of which used more highly oriented samples.[29,30] There is no indication in the MCD spectrum[29,31] of **1** that such a transition is present, either, and we suspect that the weak peak observed in the *y*-polarized absorption in ref 31 is an artifact of the type relatively frequently observed in stretched-sheet spectra.[29,37] The proposed[31] presence of a *y*-polarized transition preceding the intense *z*-polarized band at ~40 000 cm^{-1} was supported by a CNDO/S calculation including doubly excited configurations. Similar results were obtained with even more extensive CI[38] and also in our present calculation by the MNDOC method. We have now repeated the calculation of ref 31 and find that the effect of doubly excited configurations on the relative energies of the *y*-polarized and *z*-polarized transitions is only minor (2 000 cm^{-1}). Calculations in the standard PPP approximation[29] and in the LCOAO approximation[15] place the *y*-polarized transition ~4 000 cm^{-1} above the *z*-polarized one. We believe that this order is more likely correct and that the exaggerated negative value of β_{13} in the CNDO/S and MNDOC approximations causes the energy of the *y*-polarized transition to be underestimated. In our opinion, the weak *y*-polarized transition has not been convincingly observed in **1** either below or above the *z*-polarized band at ~40 000 cm^{-1}.

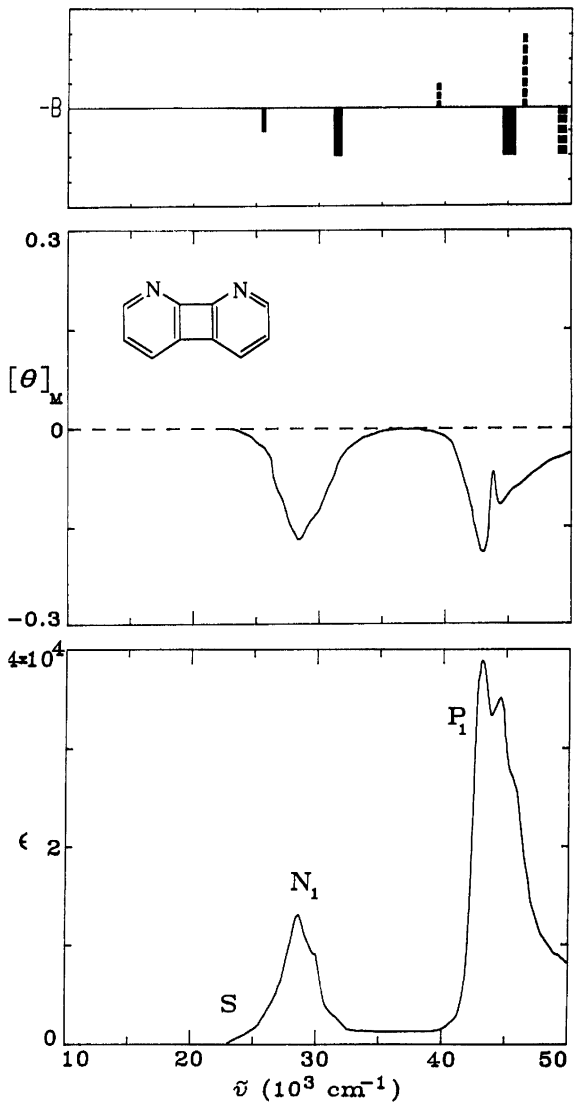

Figure 2. The absorption (bottom) and MCD (top) spectra of **1,8-N-1**, adapted from ref 31. Results of an LCOAO calculation are shown on top (see caption to Figure 1).

Much of the confidence with which the presence of a *y*-polarized transition below 40 000 cm^{-1} in **1** was proposed in ref 31 was derived from the results obtained on **1,8-N-1**, Figure 2, and **2,7-N-1**, Figure 3. In the former, and even more clearly in the latter, *y*-polarized intensity was detected in this region in the stretched-sheet spectra. In the latter, even the isotropic absorption shows a distinct shoulder at this location and there is a positive peak in the MCD. We believe, however, that these spectral features are due to an A_g state of **1**, which becomes symmetry allowed in the diaza derivatives. Such an A_g state is calculated in this spectral region by all the methods, including the most recent and best (complete active space with second-order perturbation theory, CASPT2)[33] and has been observed convincingly in the two-photon absorption spectrum.[32] We shall see in the following that the results of the perimeter model for the spectra of **1**, **1,8-N-1**, and **2,7-N-1** agree well with the observations, provided that the state ordering (i.e., a *y*-polarized transition located above 40 000 cm^{-1}) and the particular type of deviation from perfect alternant pairing symmetry that are suggested by the LCOAO model[15] are assumed.

Frontier Orbitals of 1. Figure 4 shows the Hückel approximation to the six π-symmetry frontier MOs of **1** that result from the highest doubly occupied (HO), the singly occupied

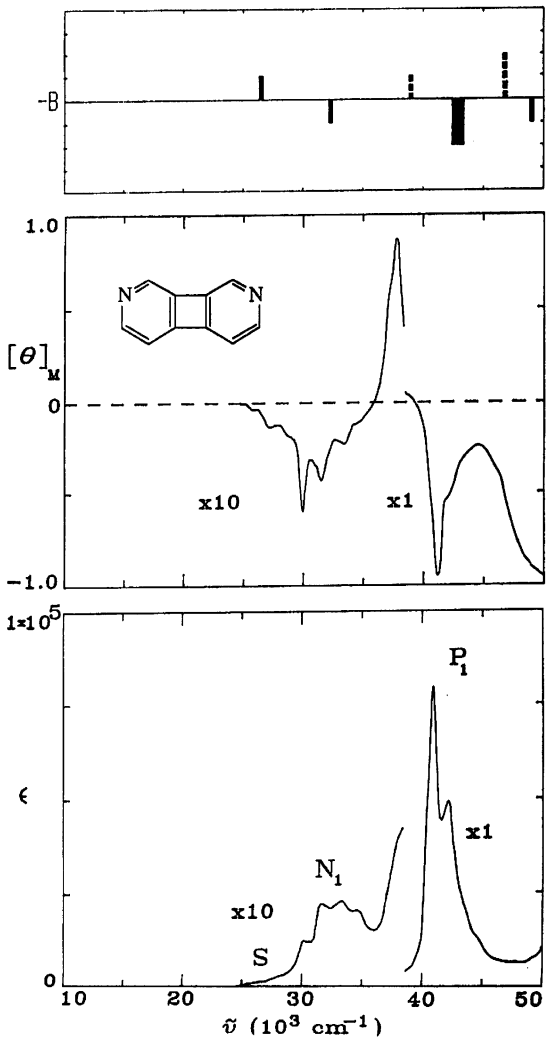

Figure 3. The absorption (bottom) and MCD (top) spectra of **2,7-N-1**, adapted from ref 31. Results of an LCOAO calculation are shown on top (see caption to Figure 1).

(SO), and the lowest unoccupied (LO) doubly degenerate orbitals of an ideal [12]annulene perimeter upon the double cross linking that produces **1**, as shown in Figure 5A. These are the six MOs that are considered in the perimeter model of parts 1−4,[1,4,8,9] and are labeled h_-, h_+, s_-, s_+, l_-, and l_+. The five singly excited states considered in the perimeter model, S, N_1, P_1, N_2, and P_2, arise as shown in Figure 5A. Figure 4 also shows the energies of two "intruder" MOs, one bonding (b_{1g}) and one antibonding (b_{2g}), that originate in lower- and higher-lying perimeter orbitals, respectively, and are ignored in the perimeter model. The description of excited states of **1** that follows will utilize the orbital and state labels introduced in Figures 4 and 5A.

Observed Spectra of 1 and its Aza Analogues (Figures 1−3). Earlier investigations[27−33] have established that **1** has at least five singlet $\pi-\pi^*$ transitions in the region below 50 000 cm^{-1} (the present computational results are collected in Tables 1−3). As noted above, one of the reported UV transitions is controversial. Additional transitions of the $\pi-\sigma^*$ and Rydberg types, and in **1,8-N-1** and **2,7-N-1**, also of the n$-\pi^*$ type, can be expected to be buried under the $\pi-\pi^*$ absorption intensity, but they have not been observed. If experience with other conjugated polycyclic hydrocarbons and their aza analogues is any guide, they will be extremely weak and will not materially affect the observed MCD spectra, either.

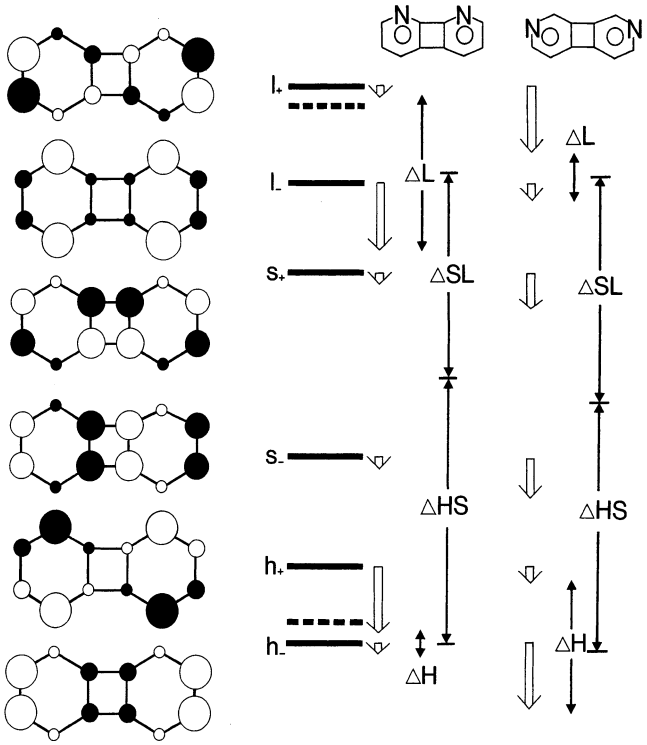

Figure 4. The Hückel MOs of **1**, their energies and perimeter labels, and the first-order effects of aza replacement. The dashed lines represent "intruder" energy levels (bonding b_{1g} and antibonding b_{2g}). These MOs originate from the next-lower and next-higher perimeter orbital pairs and play no role in the perimeter model as used here.

(i) *Transition 1.* The lowest singlet excited state of **1** is of B_{3g} symmetry. The transition from the ^1A_g ground state (G) is symmetry forbidden and appears in the absorption and MCD spectra very weakly, only due to vibronic activity.[39] There is no doubt that this transition is due primarily to the excitation of an electron from the highest occupied to the lowest unoccupied MO, $s_- \rightarrow s_+$, and the excited state is labeled S (Figure 5). Its fairly high energy, ∼24 000 cm^{-1}, implies that the allowed magnetic mixing of this state into the ground state will be able to produce only moderate contributions to the *B* terms of higher excited states. The MCD intensity of the G → S transition is very weak, negative (positive *B* term), and clearly of vibronic origin, beyond the scope of the present discussion.[40] In the aza analogues, the observed properties of this transition are almost the same, although it is no longer symmetry forbidden. This is as expected from the perimeter model.[8]

(ii) *Transition 2.* The second excited state is of B_{1u} symmetry (see formula **1** for the labeling of the axes). The G → B_{1u} transition is long-axis polarized, moderately intense, and has a positive *B* term[29] of $\sim 0.5 \times 10^{-3}$ Bohr magneton Debye^2/cm^{-1}. Its energy is ∼28 000 cm^{-1}, only a little above G → S. This transition has vanishing calculated intensity in the standard PPP approximation, and its fairly large observed oscillator strength is an additional indication that **1** does not have perfect alternant pairing properties. However, some of the intensity has been attributed to vibronic intensity borrowing through a_g vibrations.[30]

The calculated zero intensity is due to exact cancellation of the transition moment contributions provided by two dominant configurations that are of equal weight in the standard PPP model. The presence of two configurations of comparable importance agrees perfectly with the perimeter model description of parts 2[8] and 3[9] in whose terms these are the configurations $\Psi^{l_-}_{s_-}$ and $\Psi^{s_+}_{h_+}$ (Figure 5), and the transition is labeled N_1. In calculations by more advanced methods, the perfect balance is

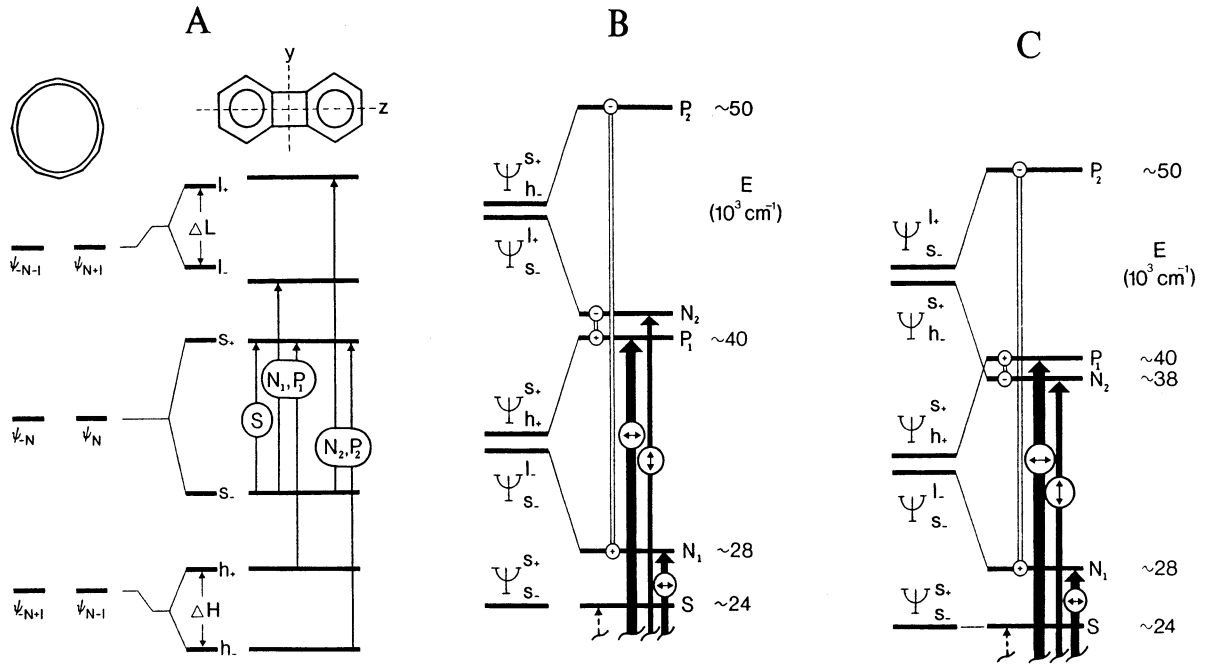

Figure 5. (A) HMO energy levels of [12]annulene (left) and **1** (center), and the five singly excited configurations responsible for the S, N_1, N_2, P_1 and P_2 states (right). (B, favored; C, possible) Two arrangements of configuration and state energies compatible with the MCD spectra of **1** using the perimeter model. See text.

lost (Tables 1−3). One of these configurations enters with a larger coefficient than the other and imposes the direction of its transition moment on the now imperfectly balanced sum. From the observed intensity alone, we cannot tell which configuration dominates, since only the square of the resultant transition moment matters.

In **1,8-N-1**, the observed G → N_1 transition is intensified relative to **1**, and its *B* term is more strongly positive (Figure 2). One can expect that in the theoretical description the perturbation by the nitrogen atoms enhances the dominance of one of the two configurations further. In contrast, in **2,7-N-1**, the observed intensity of the G → N_1 transition is reduced relative to **1**, but its *B* term is nearly unchanged (Figure 3). In these positions, the nitrogen atoms apparently reduce the dominance of the prevalent configuration in the theoretical description. We shall return to the aza derivatives of **1** in more detail below and shall find that these expectations are indeed fulfilled. The perimeter model interpretation of the MCD signs and a first-order perturbation analysis of the aza replacement effects (Figure 4) provide two mutually independent ways of reaching the conclusion that $\Psi^{l_-}_{s_-}$ is the configuration that dominates the wave function of the N_1 state. This agrees with results of our LCOAO, TD DFT, and SAC-CI calculations.

(iii) *Transition 3.* According to all methods of calculation, the third excited state is of A_g symmetry. The G → A_g transition is symmetry forbidden and unobserved in the one-photon spectrum **1** but is very intense in its two-photon spectrum. It becomes one-photon allowed and *y* polarized in both diaza analogues.

In terms of the perimeter model, this is an "intruder" state, originating in excitations involving orbitals other than those derived from the HO, SO, and LO levels of the perimeter. Its A_g symmetry permits it to mix with the D configuration of the perimeter model, which corresponds to double excitation ($\Psi^{s_+,s_+}_{s_-,s_-}$). A priori, one would expect this admixture to be small, as the latter should be quite high in energy, given the energy of the S transition. Different methods of calculation differ with regard to its relative amplitude. According to the ab initio CASPT2 method, the D configuration is stated to dominate,[33] while in our calculations, including SAC-CI, the dominant configurations are, first, a promotion from a b_{1g} orbital originating in a level below HO into s_+ (b_{1g}) and, second, a promotion from s_- (b_{2g}) into a b_{2g} orbital originating in a level above LO (the b_{1g} and b_{2g} MO levels are dashed in Figure 4). In the CNDO/S approximation, the D configuration has a weight of only about 10%. In the LCOAO and the TD DFT calculations, double excitations are not treated, and these methods offer no information on this issue.

According to the assignment preferred by us, this transition has been observed in both diaza analogues. In **1,8-N-1**, it is located near 38 000 cm^{-1}, and is submerged under the much stronger fourth transition both in ordinary absorption and in MCD spectra, but seems to appear in the *y*-polarized reduced stretched-sheet spectrum.[31] In **2,7-N-1**, this transition is shifted to lower energy and appears clearly as a shoulder in the absorption spectrum and as a distinct peak with a weakly positive *B* term in the MCD spectrum. In the assignment preferred in ref 31, it was assumed that this transition has not been observed in any of the three compounds.

(iv) *Transition 4.* The fourth excited state is of B_{1u} symmetry. This long-axis polarized transition is an order of magnitude stronger than the G → N_1 transition. It is observed near 40 000 cm^{-1} and has a positive *B* term whose magnitude has not been reported but appears to be about 5−10 times that of the transition into the N_1 state.[29] In the perimeter model, and in all calculations (Tables 1−3), from PPP to SAC-CI and CASPT2,[33] this is the intense counterpart to the G → N_1 transition, in which the contributions of the $\Psi^{l_-}_{s_-}$ and $\Psi^{s_+}_{h_+}$ configurations to the transition moments add in phase. The perimeter model label is P_1. The effects of aza replacement on the properties of this transition are small.

(v) *Transition 5.* According to the assignment preferred by us, the fifth transition, A_g → B_{2u}, has not been observed in any of the three compounds. In terms of the perimeter model, this ought to be the transition into the N_2 state, originating in the out-of-phase mixing of configurations $\Psi^{s_+}_{h_-}$ and $\Psi^{l_+}_{s_-}$. As men-

TABLE 1: LCOAO Results for $^1\pi-\pi^*$ States of Biphenylene (1)

	state[a]	sym[b]	E[c]	pol[b]	f[d]	B[e]	state function[f]
1	S	B_{3g}	25.6		0	0	$0.99\Psi^{s_+}_{s_-} + ...$
2	N_1	B_{1u}	30.7	z	0.06	+0.8	$0.79\Psi^{l_-}_{s_-} - 0.57\Psi^{s_+}_{h_+} + ...$
3		A_g	38.0		0	0	$0.65\Psi^{b2g}_{s_-} - 0.64\Psi^{s_+}_{b1g} + ...$
4	P_1	B_{1u}	41.9	z	2.06	+2.1	$0.80\Psi^{s_+}_{h_+} + 0.59\Psi^{l_-}_{s_-} + ...$
5	N_2	B_{2u}	45.8	y	0.06	−3.3	$0.91\Psi^{l_+}_{s_-} - 0.35\Psi^{s_+}_{h_-} + ...$
6		B_{3g}	48.0		0	0	$0.99\Psi^{l_-}_{h_+} + ...$
7	P_2	B_{2u}	49.2	y	0.08	−0.05	$0.81\Psi^{s_+}_{h_-} + 0.25\Psi^{b2g}_{s_-} - 0.48\Psi^{l_-}_{b1g} - ...$

[a] Perimeter state label. The D state is missing since doubly excited configurations are not included in the CI procedure. [b] Long axis, z; short axis, y; out-of-plane axis, x. [c] Energy in 10^3 cm^{-1}. [d] Oscillator strength from dipole length formula. [e] B term in 10^{-3} Bohr magneton Debye^2/cm^{-1}. [f] The bonding (b_{1g}) and antibonding (b_{2g}) intruder MO levels are defined in Figure 5.

TABLE 2: TD DFT Results for $^1\pi-\pi^*$ States of Biphenylene (1)[a]

	state[b]	sym[c]	E[d]	pol[c]	f[e]	transition weight (%)[f]
1	S	B_{3g}	24.7		0	$s_- \rightarrow s_+$ (98.7)
2	N_1	B_{1u}	29.0	z	0.07	$s_- \rightarrow l_-$ (67.1), $h_+ \rightarrow s_+$ (32.8)
3		A_g	38.3		0	$b_{1g} \rightarrow s_+$ (72.6), $s_- \rightarrow b_{2g}$ (25.7)
4	N_2	B_{2u}	39.1	y	0.0	$s_- \rightarrow l_+$ (55.7), $h_- \rightarrow s_+$ (44.0)
5	P_1	B_{1u}	39.4	z	1.05	$h_+ \rightarrow s_+$ (64.6), $s_- \rightarrow l_-$ (30.9)
6		B_{3g}	40.5		0	$h_+ \rightarrow l_-$ (92.9)
7		A_g	43.2		0	$s_- \rightarrow b_{2g}$ (46.5), $h_- \rightarrow l_-$ (39.3), $b_{1g} \rightarrow s_+$ (10.6)
8		B_{2u}	43.2	y	0.01	$b_{1g} \rightarrow l_-$ (78.7), $h_+ \rightarrow b_{2g}$ (10.2), $h_- \rightarrow s_+$ (7.4)

[a] B-P86/TZVP. [b] Perimeter state label. The D state is missing since double excitations are not included. [c] Long axis, z; short axis, y; out-of-plane axis, x. [d] Energy in 10^3 cm^{-1}. [e] Oscillator strength from dipole length formula. [f] The bonding (b_{1g}) and antibonding (b_{2g}) intruder MO levels are defined in Figure 5.

tioned in the Introduction, we believe that it lies above the P_1 state (Figure 5B), as calculated by the CASPT2 method[33] and all the methods used presently, in particular LCOAO (Table 1) and SAC-CI (Table 3), with the exception of TD DFT (Table 2), which places it very slightly below.

The very low experimental intensity of this transition is remarkable. It is reproduced correctly by the standard PPP method (perfect alternant pairing, zero intensity)[29] and by the TD DFT and SAC-CI calculations and not by the LCOAO method, which predicts an oscillator strength of 0.06, the same as for the transition into the N_1 state. As in the latter, the physical origin of the small G $\rightarrow$ N_2 transition moment is to be sought in a cancellation of the contributions from the two main excitations that compose the excited state. In this case, they are $\Psi^{s_+}_{h_-}$ and $\Psi^{l_+}_{s_-}$. These excitations have equal (PPP) or comparable (TD DFT, Table 2, and SAC-CI, Table 3) amplitudes in the calculations that produce the correct result, but $\Psi^{l_+}_{s_-}$ dominates greatly in the LCOAO wave function for N_2 (Table 1). This is apparently incorrect and illustrates a limitation of the otherwise very successful LCOAO method.

A factor that undoubtedly contributes to the relative weakness of all short-axis polarized transitions in **1** is the deviation of the molecular shape from that of the regular polygon: the contributions to the transition moment due to perimeter configurations will automatically gain an advantage of up to a factor of a little over two if they are long-axis polarized over those that are short-axis polarized, and this translates into a factor of about five in relative intensities.

(vi) *Transition 6.* A feature observed at about 45 000 cm^{-1} in the two-photon absorption spectrum[32] but absent in the ordinary absorption spectrum has been proposed[33] to correspond to a transition into an A_g state. This is attributed to the G $\rightarrow$ D (A_g) transition of the perimeter model, expected to have vanishing intensity in absorption and MCD. It is predicted for this region by numerical computations but would not be expected to be observable in a one-electron spectrum under the bands due to the allowed transitions.

(vii) *Transition 7.* A y-polarized absorption observed[31] near 46 000 cm^{-1} has been assigned[33] to a transition into the P_2 (B_{2u}) state, expected to occur at quite high energies. In the MCD spectrum, a peak with a positive B term is observed at this location. In a C-perturbed[9] perimeter, the N_1-P_1 and N_2-P_2 energy gaps should be roughly comparable when the $\Psi^{l_-}_{s_-}$, $\Psi^{s_+}_{h_+}$ and $\Psi^{s_+}_{h_-}$, $\Psi^{l_+}_{s_-}$ configuration pairs are approximately degenerate, since the off-diagonal mixing elements are the same (eq 17 in Part 3[9]). This expectation is approximately fulfilled. No

TABLE 3: SAC-CI Results for $^1\pi-\pi^*$ States of Biphenylene (1)[a]

	state[b]		sym[c]	E[d]	pol[c]	f[e]	B[f]	state function[g]
20/20	1	N_1	B_{1u}	33.4	z	0.07	0.10	$0.75\Psi^{l_-}_{s_-} - 0.52\Psi^{s_+}_{h_+} + ...$
	2	S	B_{3g}	34.5				$0.95\Psi^{s_+}_{s_-} + ...$
	3		A_g	43.7				$0.64\Psi^{s_+}_{b1g} - 0.53\Psi^{b2g}_{s_-} + 0.34\Psi^{l_-}_{h_-} + ...$
	4	P_1	B_{1u}	52.2	z	2.01	0.54	$0.56\Psi^{l_-}_{s_-} + 0.77\Psi^{s_+}_{h_+} + ...$
	5	N_2	B_{2u}	53.8	y	0.001	−0.30	$0.59\Psi^{l_+}_{s_-} - 0.57\Psi^{s_+}_{h_-} + ...$
	6		B_{3g}	55.7				$0.93\Psi^{l_-}_{h_+} + ...$
	7	P_2	B_{2u}	57.8	y	0.01	0.16	$0.45\Psi^{l_+}_{s_-} + 0.31\Psi^{s_+}_{h_-} + ...$
28/100	1	N_1	B_{1u}	30.4	z	0.07	0.11	$0.76\Psi^{l_-}_{s_-} - 0.51\Psi^{s_+}_{h_+} + ...$
	2	S	B_{3g}	30.9				$0.95\Psi^{s_+}_{s_-} + ...$
	3		A_g	40.9				$0.66\Psi^{s_+}_{b1g} - 0.53\Psi^{b2g}_{s_-} + 0.23\Psi^{l_-}_{h_-} + ...$
	4	P_1	B_{1u}	47.8	z	1.50	0.38	$0.54\Psi^{l_-}_{s_-} + 0.78\Psi^{s_+}_{h_+} + ...$
	5		B_{3g}	51.4				$0.94\Psi^{l_-}_{h_+} + ...$
	6	N_2	B_{2u}	52.0	y	0.003	−0.23	$0.71\Psi^{l_+}_{s_-} - 0.53\Psi^{s_+}_{h_-} + ...$
	7	P_2	B_{2u}	54.0	y	0.0007	0.027	$0.37\Psi^{l_+}_{s_-} + 0.50\Psi^{s_+}_{h_-} + ...$
	8	D	A_g	68.0				$0.49\Psi^{s_+,s_+}_{s_-,s_-} + 0.48\Psi^{l_-}_{h_-} + 0.48\Psi^{l_+}_{h_+} + ...$

[a] An active space of either 20/20 or 28/100 occupied/virtual MOs. [b] Perimeter state label. [c] Long axis, z; short axis, y; out-of-plane axis, x. [d] Energy in 10^3 cm^{-1}. [e] Oscillator strength from dipole length formula. [f] B term in 10^{-3} Bohr magneton Debye^2/cm^{-1}. [g] The bonding (b_{1g}) and antibonding (b_{2g}) intruder MO levels are defined in Figure 5.

TABLE 4: Orbital Energy Differences (eV) for Biphenylene (1)

	CNDO/S[a]	CNDO/S[b]	MNDOC[c]	LCOAO[d]	DFT[e]	HF[f] **1**	HF[f] **1,8-N-1**	HF[f] **2,7-N-1**
ΔHSL	3.834	2.560	1.176	0.956	0.791	1.750	3.250	1.564
ΔH	1.208	1.313	1.061	1.196	0.993	1.453	0.402	2.241
ΔL	0.248	1.182	0.842	1.340	1.525	2.292	2.625	2.075
ΔHL	0.960	0.131	0.219	−0.144	-0.532	-0.839	-2.223	0.166

[a] Reference 18. [b] Reference 19. [c] Reference 21. [d] Reference 15. [e] B-P86/TZVP. [f] DZP basis set, ref 24. In addition to results for **1**, those for **1,8-N-1** and **2,7-N-1** are also shown.

additional excited states are predicted by the simple version of the perimeter model, but all the numerical calculations predict additional $\pi-\pi^*$ states in the region above 40 000 cm^{-1}. These have not been observed so far.

The Perimeter Model and the MCD Spectrum of 1. We have already indicated how the perimeter model accounts for the absorption spectrum of **1** and will now examine how it accounts for the observed MCD signs. At the simplest level of approximation, the perturbation of the [12]annulene perimeter that produces **1** consists of a geometrical distortion and of the introduction of resonance integrals across positions 0−5 and 6−11. This is an odd perturbation in the sense of Moffitt.[2,29] In a symmetry-adapted coordinate system, **1** is therefore described by the phase angle $\sigma = \pi/2$ and the nodal planes of its MOs s_- and s_+ pass through midpoints of bonds.[1] The other phase angles defined by this perturbation[1] are $\eta = -2\pi/3$ and $\lambda = -\pi/3$. The orbitals h_- and l_- are both symmetric with respect to a vertical plane in formula **1** (see Figure 4), and the molecule belongs to case C of part 3.[9]

In the perimeter model, absorption intensities and MCD signs are dictated by orbital energy differences ΔH, ΔL, ΔHS, and ΔSL (Figures 4 and 5A), combined into the crucial quantities $\Delta HL = \Delta H - \Delta L$ and $\Delta HSL = 2(\Delta HS - \Delta SL)$, and the additional quantity $\Delta HL = \Delta H + \Delta L$.[1,8,9] The degeneracy of the perimeter orbitals ψ_k is split by the perturbation that produces the molecule in question (Figure 5A), and the energies $E(h_-)$, $E(h_+)$, $E(s_-)$, $E(s_+)$, $E(l_-)$, and $E(l_+)$ of the orbitals that result from the HO, SO, and LO pairs of perimeter MOs are used to define $\Delta H = E(h_+) - E(h_-)$, $\Delta L = E(l_+) - E(l_-)$, $\Delta HS = [E(s_+) + E(s_-)]/2 - [E(h_+) + E(h_-)]/2$, and $\Delta SL = [E(l_+) + E(l_-)]/2 - [E(s_+) + E(s_-)]/2$ and hence the quantities that determine the MCD signs.

In the Hückel approximation, alternant pairing holds perfectly and **1** is a soft chromophore, with no MCD intensity ($\Delta HL = 0$, $\Delta HSL = 0$). It is clear from the experimental data that this is an unacceptable approximation and that either ΔHL or ΔHSL or both must differ significantly from zero for reasons neglected in the ordinary Hückel and PPP models, which assume perfect alternant pairing. Table 4 lists the orbital energy differences calculated in a variety of approximations and makes it clear that they are indeed very different from zero. In all instances, we find $|\Delta HSL| > |\Delta HL|$ and conclude that the MCD spectrum of **1** should be orbital-shift dominated.[9] In the case $\Delta HL > |\Delta HSL| > 0$, which is found for all the methods of calculation listed in Table 1 with the exception of CNDO/S, the computed MO energies suggest that configuration energies follow the increasing energy order $\Psi^{l_-}_{s_-}$, $\Psi^{s_+}_{h_+}$, $\Psi^{l_+}_{s_-}$, $\Psi^{s_+}_{h_-}$ (upper center section of Figure 2 in Part 3[9]), and this is indeed found. For instance, in the LCOAO approximation, their energies are 4.39, 4.80, 5.92, and 6.32 eV, respectively.

The positive sign of ΔHSL is readily understood in terms of first-order perturbation theory[41] upon inspection of the orbitals involved (Figure 4). The negative value of the diagonal resonance integrals β_{13} in the four-membered ring will stabilize the MOs of the HO and LO levels somewhat and destabilize those of the SO level strongly. This will increase the value of ΔHS and decrease the value of ΔSL relative to those given by perfect-pairing theories, in which β_{13} is neglected. At the same level of approximation, the introduction of β_{13} will not affect the values of ΔH and ΔL much. Indeed, in the LCOAO method,[15] in which the values of β_{13} have been carefully parametrized on benzene, ΔH and ΔL remain almost equal and ΔHL is very small. The other perturbations introduced upon abandoning the perfect pairing of the standard PPP method are of lesser importance; the electronegativity of the carbon atoms that have three carbon neighbors, relative to those that have two, is increased upon introduction of penetration integrals and decreased again upon subsequent orthogonalization, and in the end all carbon OAOs have nearly the same energy. This fortunate circumstance makes it possible to predict the sense of the deviation from perfect pairing symmetry, $\Delta HSL > 0$, $\Delta HL \approx 0$, from a consideration of the β_{13} terms alone.

The MCD properties of **1** can now be derived from the perimeter model as shown in Figure 5B. The molecule is an orbital-shift dominated ($|\Delta HSL| > |\Delta HL|$) positive-hard ($\Delta HSL > 0$) MCD chromophore of type C. Algebraic formulas for its B terms given in Table 2 and eqs 27 and 28 of part 3[9] apply. Given $\Delta HL > |\Delta HSL|$, and thus the state energy pattern $E(N_1) \ll E(P_1) < E(N_2) \ll E(P_2)$, they predict the MCD sign pattern N_1, +; P_1, +; N_2, −; and P_2, +.

As shown in Figure 5A, the $s_- \rightarrow s_+$ promotion yields the forbidden S state, the $s_- \rightarrow l_-$ and $h_+ \rightarrow s_+$ promotions yield the long-axis polarized N_1 and P_1 states, and the $h_- \rightarrow s_+$ and $s_- \rightarrow l_+$ promotions yield the short-axis polarized N_2 and P_2 states. The energies of the five configurations and the effects of their mutual magnetic mixing are shown in Figure 5B. Intensities of the expected electronic transitions into the resulting states are indicated by the thickness of the arrow and the associated transition-moment directions by circled short double-headed arrows. The magnetic mixing of the S state into the ground state is expected to provide a contribution $B^{F}_{S,G}$ to the B term of each final state F, and their signs are N_1, +; P_1, −; N_2, +; and P_2, −. These quantities are expected to be small because of the large G−S gap and are not shown by any symbol in Figure 5B. Mutual magnetic mixing of the N_1 and P_2 states is expected to contribute a positive quantity $B^{N_1}_{P_2,N_1}$ to the B term of N_1, but the large N_1-P_2 energy difference will reduce its size. Similar mixing of the energetically close P_1 and N_2 states should make a strong positive contribution $B^{P_1}_{N_2,P_1}$ to the B term of P_1 and a negative contribution $B^{N_2}_{P_1,N_2} = -B^{P_1}_{N_2,P_1}$ to the B term of N_2, as indicated symbolically in Figure 5B. The contributions from N_1-N_2 and P_1-P_2 mixing should be reduced by the small magnetic moments connecting these states and are not shown. They should make a positive contribution to the B terms of N_1 and P_2 and a negative one to those of N_2 and P_1. The resulting expected positive signs for the B terms of the N_1, P_1, and P_2 states, as well as the near absence of any MCD intensity for the S band, agree well with the observations. The agreement for the P_2 state could well be fortuitous since the effects of magnetic mixing with even higher energy states are

being ignored. However, the expected negative *B* term of the N_2 transition is not observed and is clearly much smaller in absolute value than that of the P_1 transition, although they should both originate largely in N_2-P_1 magnetic mixing. It appears that the G → P_1 transition or the G → N_2 transition, or both, acquire additional positive contributions to their *B* term from magnetic mixing with even higher-energy states not included in the model. Still, the overall performance of the perimeter model in predicting the MCD signs of **1** can be judged quite satisfactory.

The Perimeter Model and Numerical Calculations. We next ask whether the account of the excited−state wave functions and of the origin of the observed MCD signs in terms of magnetic state mixing that is provided by the perimeter model is in agreement with numerical calculations. All three procedures tested, LCOAO[15] (Table 1), TD DFT[16] (Table 2), and SAC-CI[14] (Table 3), account for excitations into the states contained in the perimeter model in a way that is in overall agreement with the description provided by the model. Their description includes contributions from excitations absent in the model, such as those from the b_{1g} and into the b_{2g} intruder orbitals. Because they include the additional excitations, they also account for the presence of transitions 3 and 6, which are missing in the perimeter model. Moreover, they provide excitation energies, in quite good agreement with experiment in the case of LCOAO and TD B-P86/TZVP methods and too high in the case of the SAC−CI method, which also misorders the S and N_1 states. The SAC-CI method apparently requires a larger basis set and active space than we were able to afford.

The relative intensities are in fairly good agreement with the absorption spectrum of **1** shown in Figure 1, except that the intensity of the N_1 transition relative to the higher energy P_1 is underestimated. However, this could be due to the neglect of vibronic interactions, to which some of the N_1 intensity may be attributable.[30] Also, the intensity of the N_2 transition appears to be overestimated by the LCOAO method.

For the LCOAO and SAC-CI methods, we were able to compute also the contributions $B^F_{S,G}$ and $B^F_{I,F}$ to the *B* terms of the final states induced by magnetic mixing, and the *B* terms themselves, from a relatively short sum over states. The *B* terms computed by the two methods (Tables 1 and 3) agree in their signs, except for that of the P_2 transition, which is probably too high in energy to be calculated reliably by either method. The magnitudes are all smaller in the SAC-CI result, in worse agreement with the experimental values. The experimental signs and order of magnitude (in the units used, ∼0.5 for G → N_1 and 5−10 for G → P_1) are reproduced well, except for the troublesome G → N_2 transition, for which neither the strongly negative (LCOAO) nor the more weakly negative (SAC-CI) *B* term that is calculated is actually observed (Figure 1). In summary, the numerical calculations reproduce the signs deduced qualitatively from the perimeter model, including the one (N_2) that disagrees with the experiment.

The most critical part of the evaluation of the perimeter model against the numerical calculation is the comparison of the $B^F_{S,G}$ and $B^F_{I,F}$ contributions to each *B* term, i.e., the analysis of the origin of the MCD signs in terms of magnetic mixing of molecular states. The computed magnitudes are listed in Table 5, and their signs are seen to agree very well with those deduced above from the perimeter model, providing a validation of its qualitative use for the interpretation and prediction of MCD signs. However, the analysis of the individual contributions suggests that some of the agreement between the *B* terms derived from the perimeter model and those computed at the SAC-CI level is due to apparent accidental cancelation of higher terms in the sum. For instance, the *B* term of the P_1 transition, computed to be 0.54 in the units used in the Table, contains a contribution $B^{P_1}_{11,P_1}$ of −0.52 and a contribution $B^{P_1}_{23,P_1}$ of 0.95. The high-energy states 11 and 23 are of course missing in the perimeter model.

TABLE 5: Origin of the *B* Terms in Biphenylene (1) in Terms of Magnetic Field Mixing of Perimeter-Derived States[a]

	F[b]	B	$B^F_{S,G}$	$B^F_{N_1,F}$	$B^F_{P_1,F}$	$B^F_{N_2,F}$	$B^F_{P_2,F}$
SAC-CI	P_2	0.16	−0.01	0.02	0.13	0	0
20/20	N_2	−0.30	0.03	−0.003	−0.33	0	0
	P_1	0.54	−0.05	0	0	0.33	−0.13
	N_1	0.10	0.05	0	0	0.003	−0.02
SAC−CI	P_2	0.03	0.003	0.008	0.007	0	0
28/100	N_2	−0.23	0.07	−0.01	−0.28	0	0
	P_1	0.38	−0.06	0	0	0.28	−0.007
	N_1	0.10	0.05	0	0	0.01	−0.008
LCOAO	P_2	−0.05	−0.54	−0.24	0.82	0	0
	N_2	−3.3	1.0	−0.21	−3.9	0	0
	P_1	2.1	−0.28	0	0	3.9	−0.82
	N_1	0.8	0.35	0	0	0.21	0.24

[a] Active space of 20/20 or 28/100 occupied/virtual MOs. Contributions to the *B* term of transition G → F in 10^{-3} Bohr magneton Debye^2/cm^{-1}. $B^F_{S,G}$ is derived from the magnetic mixing of states S and G and $B^F_{I,F}$ from the magnetic mixing of states I and F. [b] Perimeter state label.

The Effect of Aza Replacement. One of the claims for the perimeter model is that it permits an easy rationalization of the effects of perturbation on the MCD *B* terms by mere inspection of the Hückel MOs of the parent chromophore.[1] In the case of **1**, the effect of aza replacement (Figures 1−3) should be understandable in terms of the first-order perturbation of its MOs by the electronegative nitrogen atoms. Figure 4 shows the Hückel MOs and the anticipated first-order shifts of their energies upon either 1,8- or 2,7-diaza replacement (white arrows). They agree with the HF orbital energy differences shown in Table 4. In the Koopmans' theorem approximation, they also are in qualitative agreement with the shifts in ionization potentials observed by photoelectron spectroscopy,[42] which also shows the presence of the intruder orbital b_{1g} (dashed line in the MO level diagram in Figure 5). **1,8-N-1** is ideally suited for an increase in the $\Delta HSL - \Delta HL$ value, since in positions $\rho = 1$ and $\rho = 8$ the squared coefficient $c^2_{\rho h_+}$ in the h_+ orbital is much larger than the squared coefficient $c^2_{\rho s_-}$ in the s_- orbital. In addition to making ΔHSL more positive, aza replacement in positions 1 and 8 will make ΔHL more negative by increasing ΔL and reducing ΔH. Both of these effects act to increase $\Delta HSL - \Delta HL$ and make **1,8-N-1** a more strongly positive-hard MCD chromophore. The predominance of $\Psi^{l-}_{s_-}$ over $\Psi^{s+}_{h_+}$ in the N_1 state should increase, and an increase both in G → N_1 absorption intensity and its already positive *B* term is expected, exactly as observed.

For similar reasons, aza replacement in positions $\rho = 2$ and $\rho = 7$ should reduce the $\Delta HSL - \Delta HL$ value, although not quite as dramatically as was the case for the 1,8 replacement. A straightforward use of $c^2_{\rho s_+} - c^2_{\rho h_+}$ as a measure of the effectiveness of the perturbation[1] yields only a fraction of the effect compared with 1,8 disubstitution, in the opposite direction. As a result, **2,7-N-1** should be an only somewhat less strongly positive-hard chromophore than **1**. A distinct reduction of the absorption intensity G → N_1 is indeed observed, while its *B* term does not change much.

These trends are again reproduced by numerical computations using the LCOAO method. The results shown in Table 6 and

TABLE 6: LCOAO Results for $^1\pi-\pi^*$ States of Symmetrical Azabiphenylenes

	state[a]	sym[b]	E[c]	pol[b]	f[d]	B[e]
1,8-N-1	S	B_1	25.6	z	0.002	+0.03
	N_1	B_1	31.5	z	0.29	+1.6
		A_1	39.5	y	0.0001	−0.002
	P_1	B_1	45.1	z	1.9	+4.5
	N_2	A_1	46.3	y	0.05	−8.2
	P_2	A_1	49.3	y	0.18	+1.0
2,7-N-1	S	B_1	26.5	z	0.002	−0.03
	N_1	B_1	32.3	z	0.02	+0.35
		A_1	39.0	y	0.03	−0.09
	P_1	B_1	42.9	z	2.0	+2.7
	N_2	A_1	46.8	y	0.07	−3.4
		B_1	49.0	z	0.02	+0.09
1,4-N-1	S	A_1	26.1	y	4×10^{-5}	−0.002
	N_1	B_1	31.2	z	0.23	+1.5
		B_1	38.3	z	0.44	+0.3
	P_1	B_1	45.8	z	1.37	+7.8
	N_2	A_1	46.5	y	0.05	−11.2
		A_1	47.9	y	0.003	−0.3
2,3-N-1	S	A_1	25.6	y	5×10^{-5}	−0.008
	N_1	B_1	31.6	z	0.02	+0.35
		B_1	38.9	z	0.004	+0.03
	P_1	B_1	42.4	z	2.0	+3.3
	N_2	A_1	46.0	y	0.09	−4.3
		A_1	48.7	y	0.005	+0.4
1,4,5,8-N-1	S	B_{3g}	26.3		0	0
	N_1	B_{1u}	31.4	z	0.5	+2.1
		A_g	40.7		0	0
	N_2	B_{2u}	47.0	y	0.03	+2.4
	P_1	B_{1u}	49.9	z	1.8	−38
	P_2	B_{2u}	50.4	y	0.5	+33
2,3,6,7-N-1	S	B_{3g}	26.5		0	0
	N_1	B_{1u}	32.9	z	3×10^{-4}	−0.04
		A_g	39.5		0	0
	P_1	B_{1u}	43.9	z	2.1	+5.9
	N_2	B_{2u}	46.5	y	0.1	−6.5

[a] Perimeter state label. The D state is missing since doubly excited configurations are not included in the CI procedure. [b] Long axis, z; short axis, y; out-of-plane axis, x. [c] Energy in 10^3 cm^{-1}. [d] Oscillator strength from dipole length formula. [e] B term in 10^{-3} Bohr magneton Debye^2/cm^{-1}.

Figures 1−3 agree well not only with the observations for the N_1 and P_1 bands but also with the behavior of the symmetry-forbidden $A_g \rightarrow A_g$ "intruder" transition just below the P_1 band, which is not accounted for in the perimeter model. In **1,8-N-1**, it remains just about as forbidden as in **1**, both in absorption and in MCD, although this is no longer demanded by symmetry. In **2,7-N-1**, it is intensified significantly, both in absorption and in MCD. This is in perfect agreement with observations. To the contrary, the other symmetry-forbidden transition (S, $A_g \rightarrow B_{3g}$) is calculated to remain without any noticeable absorption and MCD intensity in both aza analogues, despite their lower symmetry, as is indeed observed. The N_2 transition ($A_g \rightarrow B_{2u}$) is not calculated to respond much to the aza replacement, either, in agreement with the fact that it remains hidden in all three compounds. Its computed but unobserved MCD intensity is as much of a puzzle in the heterocycles as it was in **1** itself.

Comparison with SAC-CI results (Table 7) shows the expected behavior for **1,8-N-1**, but in **2,7-N-1**, the intruder transition 3 is strongly mixed with the N_2 state of the perimeter. The B terms of the S and N_1 transitions behave as expected from the perimeter model, in agreement with experiment, as does the B term of the P_1 transition in **2,7-N-1**, whose positive value is computed to originate in $B^{P_1}_{P_2,P_1}$. The negative B term of the P_1 transition in **1,8-N-1**, which disagrees with the observation, originates in mixing with higher excited states, which are apparently not calculated well.

MCD Spectra of Other Biphenylene Derivatives. Table 6 collects LCOAO predictions of the MCD spectra of several additional symmetrical aza derivatives of **1**. They agree with expectations based on the perimeter model. Previous experience with the perimeter model for aromatics[10] suggests that the effects of perturbations can often be predicted very simply and yet quite reliably even in cases where the MCD spectrum of the parent cannot be accounted for in quantitative detail. It remains to be seen whether the perimeter model works just as well for nonaromatic π systems, and the best way is to outline a few consequences and allow them to be tested in the future. Now that the interpretation of the spectrum of parent **1** has been proposed, it is a simple matter to use first-order perturbation theory[41] to make such predictions by procedures outlined in part 4[1] (cf. Figure 4). For instance, to invert the MCD sign pattern, at least for the N_1 and P_1 bands, one needs substitution with π donors in positions adjacent to the four-membered ring (1, 4, 5, 8). This should raise the energy of the orbital h_+ and affect the others much less because they have small coefficients in this position and/or are far removed in energy from the donor orbital. If carried far enough, this should make ΔHL positive and at the same time ΔHSL negative, leading to an MCD sign reversal. The MCD spectrum of a derivative such as 1,4-diaminobiphenylene would therefore be of considerable interest.

An Alternative Assignment.[31] The assignment of the weak y-polarized absorption below the P_1 band of the azabiphenylenes to the intruder $A_g \rightarrow A_g$ transition of **1**, as proposed here, is an important part of our interpretation of the MCD spectra. The alternative assignment[31] of this intensity to the N_2 transition ($A_g \rightarrow B_{2u}$) and its negative B term can still be accommodated

TABLE 7: SAC-CI Results for $^1\pi-\pi^*$ States of Diazabiphenylenes[a]

	state[b]		sym[c]	E[d]	pol[c]	f[e]	B[f]	state function[g]
1,8-N-1	1	N_1	B_1	32.5	z	0.16	0.18	$0.85\Psi^{l_-}_{s_-} - 0.33\Psi^{s_+}_{h_+} + ...$
	2	S	B_1	36.0	z	0.07	0.08	$0.93\Psi^{s_+}_{s_-} + ...$
	3		A_1	45.1	y	0.00	0.00	$0.31\Psi^{s_+}_{b1g} - 0.44\Psi^{b2g}_{s_-} - 0.40\Psi^{l_+}_{s_-} + ...$
	4	N_2	A_1	53.7	y	0.00	0.17	$0.57\Psi^{l_+}_{s_-} - 0.38\Psi^{s_+}_{h_-} + ...$
	5	P_1	B_1	55.0	z	1.31	−0.25	$0.38\Psi^{l_-}_{s_-} + 0.79\Psi^{s_+}_{h_+} + ...$
2,7-N-1	1	S	B_1	33.0	z	0.00	0.01	$0.86\Psi^{s_+}_{s_-} + ...$
	2	N_1	B_1	37.7	z	0.03	0.06	$0.67\Psi^{l_-}_{s_-} - 0.50\Psi^{s_+}_{h_+} + ...$
	3	N_2	A_1	44.5	y	0.03	−0.05	$0.71\Psi^{s_+}_{h_-} - 0.43\Psi^{b2g}_{s_-} - 0.12\Psi^{l_+}_{s_-} + ...$
	4	P_1	B_1	53.4	z	1.88	0.71	$0.61\Psi^{l_-}_{s_-} + 0.72\Psi^{s_+}_{h_+} + ...$
	5	P_2	A_1	55.7	y	0.01	−0.68	$0.71\Psi^{l_+}_{s_-} + 0.21\Psi^{s_+}_{h_-} + ...$

[a] Active space of 20/20. [b] Perimeter state label. [c] Long axis, z; short axis, y; out-of-plane axis, x. [d] Energy in 10^3 cm^{-1}. [e] Oscillator strength from dipole length formula. [f] B term in 10^{-3} Bohr magneton Debye^2/cm^{-1}. [g] Analogues of the bonding (b_{1g}) and antibonding (b_{2g}) intruder MO levels in **1**, defined in Figure 5.

by the perimeter model, but only if the configuration $\Psi^{S+}_{h\_}$ lies below and not above $\Psi^{l+}_{s\_}$ (Figure 5C). This order disagrees with all of the calculations listed in Table 1 for which these configuration energies have been computed and also with the simple inspection of the orbital energy differences in all of the calculations (the observed MCD signs would require $\Delta HL < 0$, $|\Delta HL| > |\Delta HSL|$). Although possible in principle, this appears unlikely.

A definitive resolution of the uncertainty could be reached after additional measurements. If the $A_g \rightarrow A_g$ assignment of the transition near 38 000 cm^{-1} in **1** is correct, in compounds such as **2,3-N-1**, in which the *xy* plane of symmetry is removed and *xz* preserved, this transition will be long-axis polarized, and in D_{2h} analogues such as **2,3,6,7-N-1**, it will be forbidden. If the $A_g \rightarrow B_{2u}$ assignment is right, the transition will remain short-axis polarized and will be particularly intense in **2,3,6,7-N-1** (Table 6).

Conclusions

The perimeter model of parts $1-4$[1,4,8,9] (with $\Delta HSL > 0$, such that **1** is a positive-hard chromophore, ΔHL is large, and ΔHL is small) is in qualitative agreement with the observed MCD signs of low-energy transitions and accounts for the effects of aza replacement. Moreover, it accounts for excited-state wave functions and for the origin of the MCD *B* terms in terms of magnetic state mixing in the same way as the semiempirical LCOAO and ab initio SAC-CI methods. An unresolved problem is the prediction of a significant negative *B* term for the N_2 transition just above 40 000 cm^{-1} by the perimeter model, by the LCOAO method, and by the SAC-CI calculation. Such a negative *B* term is not observed.

Specific predictions are made for the MCD spectra of other derivatives of **1** and these can be used to test the validity of the reassignment proposed for one of the weakly observed transitions, and of the perimeter model.

Acknowledgment. This paper is dedicated to Prof. H. F. Schaefer III on the occasion of his 60th birthday. The work was supported by the National Science Foundation (CHE 0140478). We are indebted to Drs. K. A. Klingensmith, J. W. Downing, Y. Wang, and Ch. Repges for help with the production of art and for some of the calculations and to Prof. G. O. Hohlneicher for providing the results of unpublished calculations.

References and Notes

(1) Part 4: Fleischhauer, J.; Michl, J. *J. Phys. Chem. A* **2000**, *104*, 7776.

(2) (a) Platt, J. R. *J. Chem. Phys.* **1949**, *17*, 484. (b) Moffitt, W. *J. Chem. Phys.* **1954**, *22*, 320, 1820.

(3) (a) Heilbronner, E.; Murrell, J. N. *Mol. Phys.* **1963**, *6*, 1. (b) Gouterman, M. *J. Mol. Spectrosc.* **1961**, *6*, 138.

(4) Höweler, U.; Downing, J. W.; Fleischhauer, J.; Michl, J. *Perkin Transactions 2*, **1998**, 1101.

(5) Michl, J. *J. Am. Chem. Soc.* **1978**, *100*, 6801.

(6) Michl, J. *J. Am. Chem. Soc.* **1978**, *100*, 6812.

(7) Michl, J. *J. Am. Chem. Soc.* **1978**, *100*, 6819.

(8) Fleischhauer, J.; Höweler, U.; Michl, J. *Spectrochim. Acta* **1999**, *55A*, 585.

(9) Fleischhauer, J.; Höweler, U.; Michl, J. *J. Phys. Chem. A* **2000**, *104*, 7762.

(10) Michl, J. *Tetrahedron* **1984**, *40*, 3845.

(11) Höweler, U.; Chatterjee, P. S.; Klingensmith, K. A.; Waluk, J.; Michl, J. *Pure Appl. Chem.* **1989**, *61*, 2117.

(12) (a) Buckingham, A. D.; Stephens, P. J. *Ann. Rev. Phys. Chem.* **1966**, *17*, 399. (b) Stephens, P. J. *J. Chem. Phys.* **1970**, *52*, 3489. (c) Stephens, P. J. *Ann. Rev. Phys. Chem.* **1974**, *25*, 201.

(13) Downing, J.; Ehara, M.; Nakatsuji, H.; Michl, J. To be published.

(14) Nakatsuji, H. In *Computational Chemistry − Reviews of Current Trends*; Lesczynski, J., Ed.; World Scientific: Singapore, 1997; Vol. 2, p 62.

(15) (a) Spanget-Larsen, J. *Croat. Chem. Acta* **1986**, *59*, 711. (b) Spanget-Larsen, J. *Theor. Chem. Acc.* **1997**, *98*, 137.

(16) Dreizler, R. M.; Gross, E. K. U. *Density Functional Theory: An Approach to the Quantum Many-Body Problem*; Springer-Verlag: Berlin, Heidelberg, 1990.

(17) Del Bene, J.; Jaffé, H. H. *J. Chem. Phys.* **1968**, *48*, 1807, 4050.

(18) Baumann, H.; Oth, J. F. M. *Helv. Chim. Acta* **1980**, *63*, 618.

(19) Dick, B.; Hohlneicher, G. *Theor. Chim. Acta* **1979**, *53*, 221.

(20) Fawcett, J. K.; Trotter, J. *Acta Cryst.* **1966**, *20*, 87.

(21) (a) Thiel, W. *J. Am. Chem. Soc.* **1981**, *103*, 1413. (b) Schweig, A.; Thiel, W. *J. Am. Chem. Soc.* **1981**, *103*, 1425.

(22) (a) Becke, A. D. *J. Chem. Phys.* **1988**, *88*, 2547. (b) Becke, A. D. *Phys. Rev.* **1988**, *A38*, 3098. (c) Perdew, J. P. *Phys. Rev.* **1986**, *B33*, 8822. (d) Perdew, J. P. *Phys. Rev.* **1986**, *B38*, 7406.

(23) Schäfer, A.; Huber, C.; Ahlrichs, R. *J. Chem. Phys.* **1994**, *100*, 5829.

(24) (a) Dunning, T. H., Jr. *J. Chem. Phys.* **1970**, *53*, 2823. (b) Dunning, T. H., Jr.; Hay, P. J. In *Methods of Electronic Structure Theory*; Schaefer, H. F., III, Ed.; Plenum Press: New York, 1977; p 1. (c) Magnusson, E.; Schaefer, H. F., III. *J. Chem. Phys.* **1985**, *83*, 5721.

(25) Frisch, M. J.; Trucks, G. W.; Schlegel, H. B.; Scuseria, G. E.; Robb, M. A.; Cheeseman, J. R.; Zakrzewski, V. G.; Montgomery, J. A., Jr.; Stratmann, R. E.; Burant, J. C.; Dapprich, S.; Millam, J. M.; Daniels, A. D.; Kudin, K. N.; Strain, M. C.; Farkas, O.; Tomasi, J.; Barone, V.; Cossi, M.; Cammi, R.; Mennucci, B.; Pomelli, C.; Adamo, C.; Clifford, S.; Ochterski, J.; Petersson, G. A.; Ayala, P. Y.; Cui, Q.; Morokuma, K.; Malick, D. K.; Rabuck, A. D.; Raghavachari, K.; Foresman, J. B.; Cioslowski, J.; Ortiz, J. V.; Stefanov, B. B.; Liu, G.; Liashenko, A.; Piskorz, P.; Komaromi, I.; Gomperts, R.; Martin, R. L.; Fox, D. J.; Keith, T.; Al-Laham, M. A.; Peng, C. Y.; Nanayakkara, A.; Gonzalez, C.; Challacombe, M.; Gill, P. M. W.; Johnson, B. G.; Chen, W.; Wong, M. W.; Andres, J. L.; Head-Gordon, M.; Replogle, E. S.; Pople, J. A. *Gaussian 98*, revision A.9; Gaussian, Inc.: Pittsburgh, PA, 1998.

(26) Ahlrichs, R., et al. TURBOMOLE, Version 5; Quantum Chemistry Group, University of Karlsruhe: Karlsruhe, Germany, 1998.

(27) (a) Farnum, D. G.; Atkinson, E. R.; Lothrop, W. C. *J. Org. Chem.* **1961**, *26*, 3204. (b) Hochstrasser, R. M.; McAlpine, R. D. *J. Chem. Phys.* **1966**, *44*, 3325. (c) Paradejordi, F.; Domingo, R.; Fernandez-Alonso, J. I. *Int. J. Quantum Chem.* **1969**, *3*, 683. (d) Zanon, I. *J. Chem Soc., Faraday Trans. 2* **1973**, *69*, 1164. (e) Vogler, H.; Ege, G. *J. Am. Chem. Soc.* **1977**, *99*, 4599. (f) Lin, H.-B.; Topp, M. *Chem. Phys. Lett.* **1979**, *64*, 452. (g) Okta, N.; Fujita, M.; Baba, H.; Shizuka, H. *Chem. Phys.* **1980**, *47*, 389.

(28) Wirz, J. In *Excited States in Organic Chemistry and Biochemistry*; Pullman, B., Goldblum, N., Eds.; D. Reidel Publishing Co.: Dordrecht, Holland, 1977; p 283.

(29) Jørgensen, N. H.; Pedersen, P. B.; Thulstrup, E. W.; Michl, J. *Int. J. Quant. Chem.* **1978**, *S12*, 419.

(30) Hoshi, T.; Yamamoto, H.; Miyauchi, T.; Mori, S.; Kobayashi, M.; Tanizaki, Y. *Ber. Bunsen−Ges.* **1982**, *86*, 330.

(31) Yamaguchi, H.; Ata, M.; McOmie, J. F. W.; Barton, J. W.; Baumann, H. *J. Chem. Soc., Faraday, Trans. 2* **1983**, *79*, 599.

(32) (a) Bich, V. T.; Bini, R.; Salvi, P. R.; Marconi, G. *Chem. Phys. Lett.* **1990**, *175*, 413. (b) Gellini, C.; Salvi, P. R.; Orlic, N. *Chem. Phys. Lett.* **1995**, *246*, 335.

(33) Beck, M. E.; Rebentisch, R.; Hohlneicher, G.; Fülscher, M. P.; Serrano-Andrés, L.; Roos, B. O. *J. Chem. Phys.* **1997**, *107*, 9464.

(34) Michl, J. *J. Chem. Phys.* **1974**, *61*, 4270.

(35) (a) Coulson, C. A.; Rushbrooke, G. S. *Proc. Cambridge Phil. Soc.* **1940**, *36*, 193. (b) Pariser, R. *J. Chem. Phys.* **1956**, *24*, 250. (c) McLachlan, A. D. *Mol. Phys.* **1961**, *4*, 49. (d) Koutecký, J. *J. Chem. Phys.* **1966**, *44*, 3702. (e) Živković, T. P. *Croat. Chem. Acta* **1984**, *57*, 367, 1553.

(36) (a) Ellis, R. L.; Jaffé, H. H. *J. Mol. Spectrosc.* **1974**, *50*, 474. (b) Jørgensen, P.; Poulsen, J. C. *J. Phys. Chem.* **1974**, *78*, 1420. (c) Obbink, J. H.; Hezemans, A. M. F. *Chem. Phys. Lett.* **1977**, *50*, 133.

(37) Michl, J.; Thulstrup, E. W. *Spectroscopy with Polarized Light*; VCH Publishers: Deerfield Beach, FL, 1986; pp 230, 267, 403.

(38) Hohlneicher, G. Private communication.

(39) Marconi, G. *Chem. Phys. Lett.* **1990**, *169*, 617.

(40) Zgierski, M. Z. *J. Chem. Phys.* **1985**, *83*, 2170; **1986**, *85*, 109.

(41) Dewar, M. J. S.; Dougherty, R. C. *The PMO Theory of Organic Chemistry*; Plenum Press: New York, 1975.

(42) Yamaguchi, H.; Higashi, M.; MacBride, J. A. H.; Gleiter, R. *J. Chem. Soc., Faraday Trans. 2* **1985**, *81*, 1831.